

COMMUNICATION

[View Article Online](#)  
[View Journal](#)



Cite this: DOI: 10.1039/d4mr00086b

Received 31st July 2024  
Accepted 15th October 2024

DOI: 10.1039/d4mr00086b

[rsc.li/RSCMechanochem](http://rsc.li/RSCMechanochem)

The failure of interfaces between polymers and inorganic substrates often leads to deteriorated performance, as is the case for polymer matrix composites. Interfacial mechanophores (iMPs) have the potential to fluorescently measure interfacial failures. Spirolactam-based mechanophores are of interest due to their readily available synthetic precursors and compatibility with epoxy matrices. In this work, spiro lactam is covalently bound at the interface of silica surfaces and epoxy, chosen due to the industrial relevance of glass fiber composites. The iMPs are mechanically activated through uniaxial tension applied to the composite while the resulting fluorescent response is observed *in situ* with a confocal microscope. Due to their real time sensing capabilities, iMPs are a promising technique to measure interfacial failures in composite materials more easily than with traditional optical microscopy techniques.

Lightweight polymer composites have become a large part of the structural world around us due to their high specific strength (strength per unit weight). However, unlike traditional metallic materials which have measurable indications of impending failure, composites can fail immediately and catastrophically with little to no warning.<sup>1,2</sup> This extreme failure mechanism requires higher safety factors, often resulting in a shortened service life. Interfacial failure of the respective components is where composite materials commonly fail. Other materials prevalent in today's society which are also susceptible to debonding of polymeric materials are structural

adhesives, microchip encapsulants, and protective coatings.<sup>3-6</sup> By establishing a better understanding of the interfacial failure mechanisms, interfacial mechanophores (iMPs) could detect early warning signs of failure at smaller separation distances, enabling products to remain in service longer, thus reducing excess waste.

Characterization techniques to measure material interfaces have traditionally been *ex situ*, postmortem analyses which investigate fractured surfaces in specimens that have already failed. Many current techniques to measure interfacial failure rely on optical microscopy and are therefore limited in their detection of separation distances of interfacial failures by the diffraction limit of light (approximately 250 nm). Ultrasound and X-ray are non-destructive techniques commonly used to measure the structural integrity of material by detecting flaws and failures such as air bubbles and delaminations with larger lateral dimensions.<sup>1</sup> Separation distances below the nanometer length scale are undetectable through traditional techniques and require other approaches to identify their locations.

One type of molecular scale sensor with the potential to highlight sub-nanometer interfacial separations is a mechanophore. Mechanophores are a class of stimuli responsive molecules that undergo a structural change when subjected to an externally applied force.<sup>7</sup> The structural rearrangement results in a change in optical or catalytic properties.<sup>7,8</sup> From an optical standpoint, the molecule transitions from a nonfluorescent, inactive state to a fluorescently active state. In solution, mechanophores can be activated through sonication. When embedded in polymeric materials, stresses are transmitted through the extension of polymer chains to the mechanophores, leading to activation. The stress transfer allows for the observation of stress localization and quantification within a polymer matrix using mechanophore fluorescence intensity.<sup>9-13</sup> One of the first reported mechanophores was spirocyclic and was covalently embedded in a poly(methyl acrylate) matrix.<sup>14,15</sup> Since then, over twenty different mechanophore molecules have been referenced in literature.<sup>16,17</sup>

<sup>a</sup>School of Materials Engineering, Purdue University, West Lafayette, Indiana, 47906 USA

<sup>b</sup>School of Chemical Engineering, Purdue University, West Lafayette, Indiana, 47906 USA

<sup>c</sup>Department of Material Science and Engineering, University of Delaware, Newark, Delaware, 19716 USA. E-mail: [ChelseaD@UDel.edu](mailto:ChelseaD@UDel.edu)

<sup>d</sup>Air Force Research Laboratory, Materials and Manufacturing Directorate, Wright-Patterson AFB, Ohio, 45433 USA

<sup>e</sup>Department of Mechanical Engineering, University of Delaware, Newark, Delaware, 19716 USA

† Electronic supplementary information (ESI) available. See DOI: <https://doi.org/10.1039/d4mr00086b>



iMPs are an emerging technology that allows for the detection of interfacial separations on the order of nanometers.<sup>18</sup> Mechanophores are covalently attached at the interface between two materials, rather than embedding the mechanophores within the bulk of a polymer material. A maleimide–anthracene mechanophore covalently attached to a silica nanoparticle and poly(methyl acrylate) was the first example of a covalently attached iMP.<sup>19</sup> Through sonication of the silica nanoparticles in a suspension, the mechanophores were activated. Years later, the same anthracene-derived mechanophores were localized at the interface of a silicon wafer and an epoxy encapsulant, mimicking a microchip interface.<sup>18</sup> Using laser-induced stress waves, the mechanophores were activated. This activation was then measured using an epifluorescence microscope after debonding.

As the original mechanophore, spiropyran has been studied extensively in bulk polymer applications.<sup>10,14,20–26</sup> However, some recent work has focused on utilizing spiropyran as an interfacial mechanophore. Grady *et al.* attached spiropyran to fiberglass fibers and conducted microbond interfacial shear testing experiments to observe mechanophore activation.<sup>27</sup> By functionalizing silica nanoparticles with interfacial spiropyran, Kim *et al.* were able to increase the stress sensitivity of their spiropyran mechanophores in acrylate nanocomposites.<sup>28</sup>

While spiropyran has been used in many academic studies, it can be difficult to synthesize and has only recently become available commercially. Alternatively, spirolactam (SPL) mechanophores are of particular importance due to the commercial availability of their synthetic precursors and their chemical compatibility with industrially relevant epoxy resins. Preliminary studies have focused on embedding SPL mechanophores into bulk epoxy systems.<sup>29</sup> To detect surface scratches in glassy epoxy systems, SPL was used and remained fluorescently active for periods of over 1200 h. In single fiber composite systems, SPL mechanophores were used to visualize the matrix failure around the composite as well as the changes in fluorescence lifetime during fracture.<sup>30</sup> As an iMP, spirolactam has been covalently bonded between silk fibers and an epoxy network, and activation was detected upon deformation of the composite.<sup>31</sup> The rhodamine 110 precursor was covalently attached to the fiber surface through the pendant amine functionality. In that study, the functionalized silk fiber/epoxy samples were strained in uniaxial tension and the mechanophore activation was measured *ex situ*.

In this work, we relate interfacial failure to mechanical activation of spirolactam mechanophores at the interface of industrially relevant synthetic materials (Fig. 1). Silica spheres are functionalized with various silanes and SPL molecules are then reacted to the silanes. Individual spheres are then embedded in a two-part thermoset matrix. Single-particle composite samples are measured *in situ* by applying uniaxial tension while observing the fluorescence intensity of the activation over an inverted confocal microscope. Activation of interfacial mechanophores is reported here for the first time using commercially available dye molecules (rhodamine 110) on glass/epoxy composites. The implications of this study are wide-ranging and could have a significant impact on composite

structural health monitoring as well as possible applications in the detection of nanometric separations of protective coatings and microchip encapsulants.

Precise control of the interfacial strength through the extent of the covalent attachment between the silica and epoxy was required for this study. Three types of surfaces were prepared (Fig. 1b). For all three surfaces, clean silica substrates were first functionalized with hexyltriethoxysilane (HTEOS) and *N*-(6-aminoethyl)aminomethyltriethoxysilane (AHAMTEOS) to silanize the silica particles, forming an amine-functionalized control (C-NH<sub>2</sub>). Details of the synthesis are provided in the ESI (S1†). To enhance the detection of iMP activation, we intentionally weakened the silica particle–epoxy interface and selected an epoxy system with a lower glass transition temperature ( $T_g$ ). High  $T_g$  epoxy systems have higher moduli, resulting in relatively small ultimate strains at failure. This small deformation complicates measurements of interfacial separation, as the crack front propagates too quickly for localized stress transfer to be adequately visualized. By lowering the  $T_g$ , we reduce the matrix stiffness near the interface, allowing for more gradual stress transfer. Additionally, a weakened interface ensured interfacial failure rather than matrix failure. We weakened the silica particle–epoxy interface by incorporating HTEOS on the silica surface. The SPL mechanophore (using rhodamine 110 as a precursor) was covalently bonded to the silane-functionalized silica spheres, I-SPL (S2, ESI†). Control samples, C-SPL, were synthesized to test if frictional activation of SPL occurred (Fig. 1b(ii)). C-SPL molecules were synthesized using rhodamine B as a precursor which prevented covalent bonds to the polymer matrix due to the terminal, nonreactive ethyl groups on the aromatic amines of rhodamine b (S3, ESI†).

The functionalized silica spheres were embedded into the curing epoxy matrix to create covalent bonds between the iMP and the epoxy network (S4, ESI†). For the epoxy in this study, the selected monomer was diglycidyl ether of bisphenol A (DGEBA) with polyetherdiamines as the crosslinkers. Upon the application of force along the molecule, the iMP isomerizes to a fluorescently active state. Here, we apply uniaxial tension to the single particle containing specimen, mimicking a stress distribution experienced in particle reinforced composites. *In situ* mechanical SPL activation was observed through confocal fluorescence microscopy, indicating interfacial load transfer from the matrix to the particle.

To monitor the extent of surface functionalization, Fourier-transform infrared (FTIR) spectroscopy was used. Beginning with untreated silica, planar surfaces were measured after each step in the process. As shown in Fig. 2, the untreated silica has minimal absorption in the region of interest (1500–2000 cm<sup>−1</sup>). The addition of HTEOS and AHAMTEOS to the surface of the glass produced an increased absorption in the 3800 cm<sup>−1</sup> region from the AHAMTOES amines and in the 3000 cm<sup>−1</sup> region from added –CH stretches from both AHAMTOES and HTEOS. The addition of SPL's aromatic rings to the silica surface was confirmed by absorption near 1700 cm<sup>−1</sup>, the aromatic region. The change in appearance in the amine region, 3800 cm<sup>−1</sup>, along with the new peaks in the aromatic region of



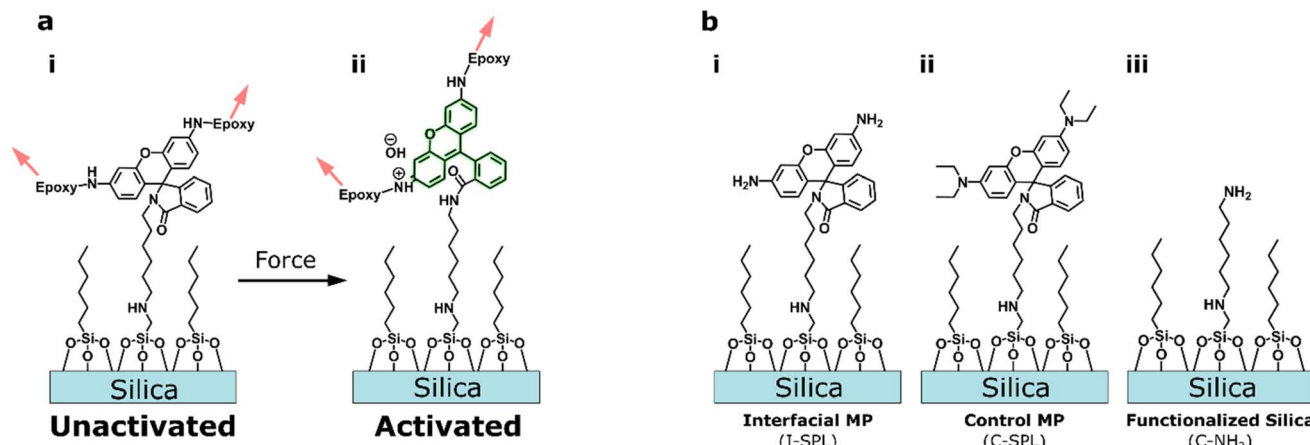


Fig. 1 (a) Activation of covalently bonded spirolactam (SPL) and epoxy through mechanical loading. (b) Chemical structures of synthesized functional silica surfaces. I-SPL is mechanically active and has covalent bonds with the epoxy and silica surface. C-SPL has a SPL mechanophore covalently bonded to the silica surface but not covalently bonded with the epoxy to test for frictional activation. C-NH<sub>2</sub> is the amine-terminated silane functionalized surface and allows for covalent bonds between the epoxy and the silica surface for mechanical properties comparison between composite specimens with and without interfacial mechanophore (iMP).

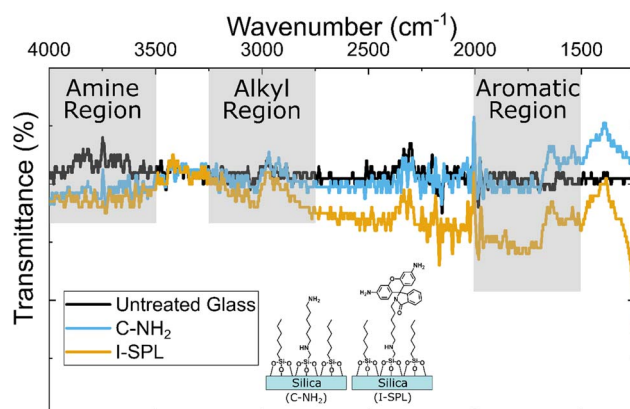


Fig. 2 Surface functionalization monitored by infrared spectra. Additional absorption at 1700 cm<sup>-1</sup> due to the presence of aromatic rings in SPL is observed.

the FTIR confirms the covalent attachment of the SPL to the interface of the silica.

To measure the mechanical response of the iMP, dogbone tensile specimens were prepared containing a single iMP-functionalized particle. Custom grips were outfitted on the load frame to allow for observation of the sample with a confocal microscope during each tensile experiment. Samples were strained in uniaxial tension over a laser scanning confocal microscope to record *in situ* fluorescence measurements (Fig. 3). Further details of these experiments and the precise testing conditions have been reported previously.<sup>9,12</sup>

For each *in situ* mechanical test, stress *versus* strain curves were obtained, synchronized with a time lapse image sequence of the fluorescence activation. As shown in Fig. 4a, I-SPL does not significantly change the mechanical response compared to that of C-NH<sub>2</sub>. The initial modulus taken from the linear portion of the stress-strain graph is about 0.01 MPa for all

materials. The iMP functionalized particles have moderate adhesion with the matrix due to the mixture of bonding and nonbonding silanes on the surface of the particle. The matrix remains attached to the iMP functionalized particle for the majority of the deformation until, at approximately 100% strain, the matrix detaches in a Gent-Park style debonding event.<sup>32</sup> The deformation can be visualized in Fig. 4b with the detachment noticeable in (iii).

Fluorescence images of an iMP-functionalized particle (Fig. 4c(i)–(iv)) demonstrate the capability of this system to indicate interfacial separations on the nanometer length scale which are not readily observable with conventional brightfield optical microscopy. Interfacial stress transfer from the matrix to the silica particle is shown at 40% strain in the iMP-functionalized composite. The increasing fluorescence intensity with additional strain indicates stress transfer occurring

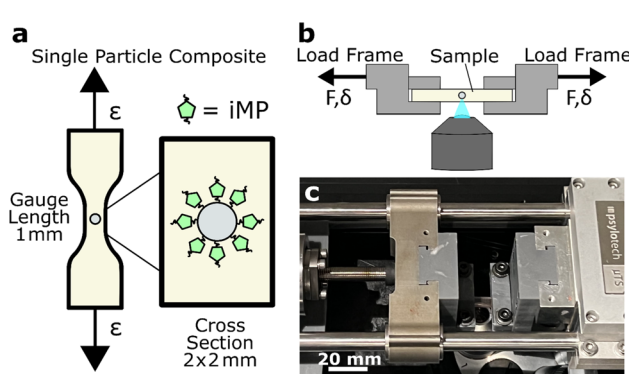


Fig. 3 (a) Uniaxial tensile test sample geometry. Single particle composite specimens were fabricated with the particle located at the sample centroid. (b) Samples were strained over a laser scanning confocal microscope to measure the interfacial mechanophore activation *in situ*. (c) A photograph of the experimental setup for the *in situ* confocal microscopy during tensile tests.



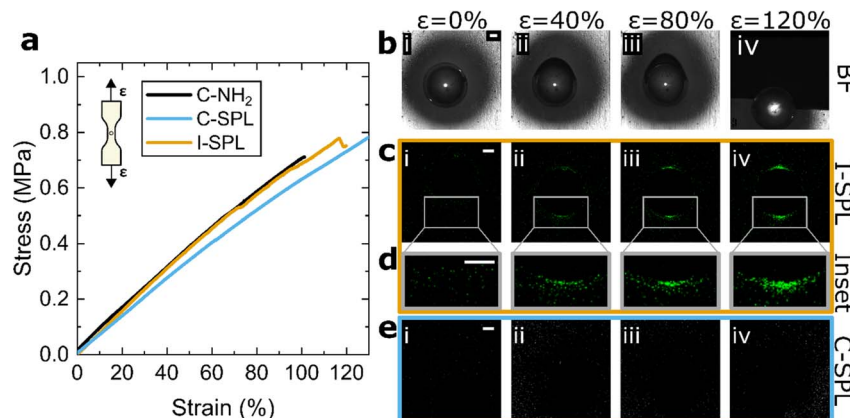


Fig. 4 (a) Stress versus strain of the single particle samples during uniaxial tensile testing. The three different silica/epoxy interfaces are indicated in the legend. (b) Brightfield images of the damage of a single particle composite system. (c) *In situ* confocal microscopy images of the I-SPL samples at 0, 40, 80, and 120% strain with insets shown in (d). (e) Equivalent strains are shown for C-SPL. In all images (b–e), scale bars represent 100  $\mu$ m and apply across each row (i–iv). Strains are marked at the top of each column of images. The images in (b–e) were captured during three different experiments.

across the interface. iMP activation is observed at both the top and bottom poles of the particles but not necessarily to the same degree, as indicated when the comparison of fluorescence intensity with strain plotted for the two hemispheres (Fig. S5, ESI<sup>†</sup>), indicating slight differences in interfacial stress transfer. In our previous work and in several experiments in this study, Gent–Park debonding was observed at one pole or the other of the glass particle.<sup>9,12,32</sup> For example, debonding occurred on the top hemisphere during the brightfield experiment shown in Fig. 4b(iii). This interfacial failure is further proof that the strength of the bond can vary spatially around the particle surface and the iMPs are sensitive to these subtle variations. The insets of the lower half of the particle/epoxy interface during testing (Fig. 4d) help to show the sensitivity of the technique. There is a gradient in mechanophore activation intensity starting at the top and bottom poles of the sphere and migrating around the sphere surface towards the sphere's equator as additional strain is applied to the composite. The ability to observe the localization of interfacial stress transfer from matrix to reinforcement due to higher in specific locations around the particle is crucial for understanding interfacial failure in composites. The increased fluorescent activation of the I-SPL as the strain increases demonstrates the spatial resolution to show deformation at the interface of the glass bead and the epoxy matrix.

Fluorescence measurements were also taken for uniaxial tensile tests on C-SPL samples. The mechanical response of C-SPL specimens was slightly lower, indicating a small effect on the stiffness of the composite. As these control samples are unable to covalently bond with the epoxy matrix, activation is not observed, even at large strains as observed in Fig. 4e. The lack of mechanophore activation demonstrates that SPL does not undergo friction-caused activation. C-SPL was chosen to demonstrate that the fluorescence seen with I-SPL is a damage indicator accessed by a force pathway through the covalent bonds breaking the sacrificial spirolactam bond.

To further quantify the fluorescence activation of the iMPs in this study, image analysis was conducted of interfacial activation at increasing strains (SV1, ESI<sup>†</sup>). Activation occurred along the particle surface and the intensity of the activation increased as the interfacial stress transfer increased with increasing strain, activating more and more iMP molecules (Fig. 5a). A region of interest (ROI) ranging from the particle's center to 350  $\mu$ m along the direction of loading with a width of 15  $\mu$ m was defined, and the fluorescence intensity was plotted. The intensity peaked just past the particle surface ( $r = 200 \mu$ m, indicated with the vertical dotted line). Stress transfer around the particle surface was observed by measuring the activation angle,  $\theta_A$ , defined as the angle from the vertical axis to where activation was first observed (Fig. 5b). By plotting the average  $\theta_A$  of the four angles, shown in the inset, the interfacial stress can be tracked around the poles of the particle, as a function of strain. Around 20% strain, the  $\theta_A$  began to increase as more of the interface was placed in tension. Our ability to spatially observe interfacial stress is apparent through this analysis.

The average intensity was then quantified as a function of position along the particle surface for each ROI, shown schematically in the inset of Fig. 5c. The decrease in activation for the ROI demonstrates further with the increase in angle away from the direction of loading there is less iMP activation (Fig. 5c). More details about image analysis can be found in ESI (S6<sup>†</sup>). All fluorescence intensity image analysis performed supports the sensitivity of the iMP for stress analysis in micron length scale.

This analysis builds on our previous work with MP-functionalized polymer matrices, where bulk activation revealed stress distribution across the matrix and Gent–Park cavitation and debonding on one side of the particle.<sup>9,32</sup> Here, the use of iMPs at the polymer–inorganic interface provides more localized insights into interfacial stress transfer mechanisms. The fluorescence intensity profiles in Fig. 5 show that, like in the bulk matrix, local stress can be unevenly distributed.



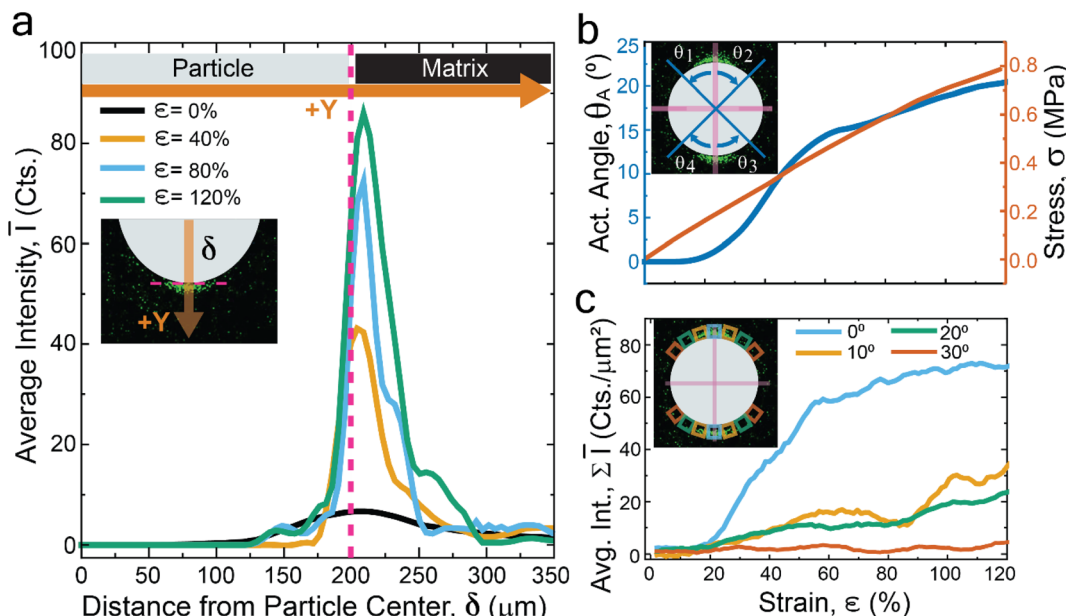


Fig. 5 Image analysis of iMP activation during tensile loading. (a) Average intensity,  $\bar{I}$ , as a function of distance from the particle center,  $\delta$ , to 350  $\mu\text{m}$  in the direction of loading. The graph inset describes the positive direction relative to the particle's center. (b) Activation angle,  $\theta_A$ , (left y-axis) and stress,  $\sigma$ , (right y-axis) as a function of strain,  $\epsilon$ . The graph inset describes the angles averaged to calculate  $\theta_A$ ,  $\theta_A = (\sum \theta_x)/4$ . (c) Average intensity,  $\sum \bar{I}$ , at various angles along the particle's surface as a function of strain,  $\epsilon$ . The graph inset describes the regions of interest used to calculate  $\sum \bar{I}$ ,  $\bar{I}_{x^\circ} = (\sum \bar{I}_{x^\circ}/n)$  for  $x = 90^\circ$ ;  $n = 2$ , for  $x^\circ = 10^\circ, 20^\circ$ , and  $30^\circ$ ;  $n = 4$ . For illustrative purposes, the image obtained at 120% strain was used in all schematics with a particle radius of  $r = 200 \mu\text{m}$ . The x-axis scale in (c) applies to both (b and c).

The angular dependence of activation, as shown in the stress and activation angle plot, confirms that iMPs respond more intensely as additional stress is applied to the matrix and subsequently across the composite interface.

Interfacial mechanophores, like bulk mechanophores, provide a detailed picture of stress localization but with improved sensitivity at the interface. Spirolactam iMPs are demonstrated here in a commonly used set of composite materials: glass and epoxy. As proof of concept, we have shown that iMPs can be installed at interfaces without significantly changing the properties of the interface and used to subsequently visualize fluorescence intensity when sufficient stress is transferred across the interface. Further, we have demonstrated our ability to observe this fluorescence activation in real time as stress is transferred through the interface within these composites. By detecting interfacial stress buildup in real time, iMPs act as early indicators of impending failure in composite materials, especially in cases of interfacial debonding. This ability to identify failure points before they lead to catastrophic failures results in more durable composite structures, enhancing material efficiency and sustainability.

In this work, we covalently attached spiro lactam mechanophores at the interface between industrially relevant epoxy and silica surfaces. The synthesis was confirmed using infrared spectroscopy. Model composite single particle specimens were fabricated with these interfacial spiro lactams on spherical silica particles in an epoxy matrix. These samples were tested in uniaxial tension to failure and spiro lactam activation was measured *in situ* using a confocal microscope. We demonstrate

that SPL is a viable interfacial mechanophore that achieves activation through mechanical force applied to the composite matrix. The activation force required needs to be tuned to that of the adhesive strength of the interface being investigated. Additionally, this is one of the first times the activation of an interfacial mechanophore has been observed *in situ*. Building on this proof of concept, future work in this space will focus on developing a deeper understanding of the interfacial strength relationship with iMP activation as we shift to even more industrially relevant systems. Higher modulus engineering epoxies and planar or fibrillar surfaces offer routes to extend this technology into a real-world tool.

## Data availability

The data supporting this article have been included as part of the ESI.<sup>†</sup>

## Conflicts of interest

There are no conflicts of interest.

## Acknowledgements

The authors would like to thank the NSF-CMMI CAREER (Grant #2045908) and the Semiconductor Research Corporation (SRC Project #2878.013) for funding JG as well as the Air Force Research Laboratory Summer Faculty Fellowship Program for providing an internship opportunity for JG and CD during the summer of 2020. We acknowledge the NSF-NRT-MIDAS (Award

#2125703) for funding for AF. The authors would also like to thank Patrick Thompson and Monali Basutkar for serving as industrial liaisons and offering helpful guidance and feedback for the duration of the SRC funding. Distribution A cleared for public release; distribution unlimited (2024-ARFL-5903).

## References

- 1 M. G. R. Sause, *In Situ Monitoring of Fiber-Reinforced Composites Theory, Basic Concepts, Methods, and Applications*, 2016.
- 2 N. Zimmermann and P. H. Wang, *Eng. Failure Anal.*, 2020, **115**, 104692.
- 3 D. Dillard, *Advances in Structural Adhesive Bonding*, Woodhead Publishing, 2nd edn, 2023.
- 4 J. C. Whitaker, Semiconductor Failure Modes, in *Electronic Systems Maintenance Handbook*, CRC Press, 2nd edn, 2017, ch. 13.
- 5 C. Fan, Y. Liu, X. Yin, J. Shi and K. Dilger, *ACS Omega*, 2021, **6**, 20331–20340.
- 6 B. Ramezanzadeh, A. Ahmadi and M. Mahdavian, *Corros. Sci.*, 2016, **109**, 182–205.
- 7 N. Deneke, M. L. Rencheck and C. S. Davis, *Soft Matter*, 2020, **16**, 6230–6252.
- 8 D. W. Kim, G. A. Medvedev, J. M. Caruthers, J. Y. Jo, Y.-Y. Won and J. Kim, *Macromolecules*, 2020, **53**, 7954–7961.
- 9 M. L. Rencheck, B. T. Mackey, Y.-Y. Hu, C.-C. Chang, M. D. Sangid and C. S. Davis, *Adv. Eng. Mater.*, 2022, **24**, 2101080.
- 10 Y. Chen, C. J. Yeh, Q. Guo, Y. Qi, R. Long and C. Creton, *Chem. Sci.*, 2021, **12**, 1693–1701.
- 11 E. Ducrot, Y. Chen, M. Bulters, R. P. Sijbesma and C. Creton, *Science*, 2014, **344**, 186–189.
- 12 J. A. Gohl, T. J. Wiley, H.-C. Chang, C.-C. Chang and C. S. Davis, *Frontiers in Soft Matter*, 2023, **3**, 1125163.
- 13 N. Haque, J. Gohl, C.-C. Chang, H. C. Chang and C. S. Davis, *Macromol. Chem. Phys.*, 2023, **224**, 2300298.
- 14 S. L. Potisek, D. A. Davis, N. R. Sottos, S. R. White and J. S. Moore, *J. Am. Chem. Soc.*, 2007, **129**, 13808–13809.
- 15 D. A. Davis, A. Hamilton, J. Yang, L. D. Cremar, D. Van Gough, S. L. Potisek, M. T. Ong, P. V. Braun, T. J. Martínez, S. R. White, J. S. Moore, N. R. Sottos, D. A. Davis, A. Hamilton, J. Yang, L. D. Cremar, D. Van Gough, S. L. Potisek, M. T. Ong, P. V. Braun, T. J. Martínez, S. R. White, J. S. Moore and N. R. Sottos, *Nature*, 2009, **459**, 68–72.
- 16 Y. Chen, G. Mellot, D. v. Luijk, C. Creton and R. P. Sijbesma, *Chem. Soc. Rev.*, 2021, **50**, 4100–4140.
- 17 J. Li, C. Nagamani and J. S. Moore, *Acc. Chem. Res.*, 2015, **48**, 2181–2190.
- 18 J. Sung, M. J. Robb, S. R. White, J. S. Moore and N. R. Sottos, *J. Am. Chem. Soc.*, 2018, **140**, 5000–5003.
- 19 J. Li, T. Shiraki, B. Hu, R. A. E. Wright, B. Zhao and J. S. Moore, *J. Am. Chem. Soc.*, 2014, **136**, 15925–15928.
- 20 Q. Wang, G. R. GrossWeiler, S. L. Craig and X. Zhao, *J. Mech. Phys. Solids*, 2015, **82**, 320–344.
- 21 G. I. Peterson, M. B. Larsen, M. A. Ganter, D. W. Storti and A. J. Boydston, *ACS Appl. Mater. Interfaces*, 2014, **7**, 577–583.
- 22 C. M. Degen, P. A. May, J. S. Moore, S. R. White and N. R. Sottos, *Macromolecules*, 2013, **46**, 8917–8921.
- 23 A.-D. N. Celestine, B. A. Beiermann, P. A. May, J. S. Moore, N. R. Sottos and S. R. White, *Polymer*, 2014, **55**, 4164–4171.
- 24 Z. Xia, V. D. Alphonse, D. B. Trigg, T. P. Harrigan, J. M. Paulson, Q. T. Luong, E. P. Lloyd, M. H. Barbee, S. L. Craig, Z. Xia, V. D. Alphonse, D. B. Trigg, T. P. Harrigan, J. M. Paulson, Q. T. Luong, E. P. Lloyd, M. H. Barbee and S. L. Craig, *Molecules*, 2019, **24**, 542.
- 25 Y. Lin, M. H. Barbee, C.-C. Chang and S. L. Craig, *J. Am. Chem. Soc.*, 2018, **140**, 15969–15975.
- 26 M. Li, Q. Zhang, Y.-N. Zhou and S. Zhu, *Prog. Polym. Sci.*, 2018, **79**, 26–39.
- 27 M. E. Grady, C. M. Birrenkott, P. A. May, S. R. White, J. S. Moore and N. R. Sottos, *Langmuir*, 2020, **36**, 5847–5854.
- 28 T. A. Kim, C. Lamuta, H. Kim, C. Leal and N. R. Sottos, *Adv. Sci.*, 2020, **7**, 1903464.
- 29 C. S. Davis, M. L. Rencheck, J. W. Woodcock, R. Beams, M. Wang, S. Stranick, A. M. Forster and J. W. Gilman, *ACS Appl. Mater. Interfaces*, 2021, **13**, 55498–55506.
- 30 J. W. Woodcock, R. J. Sheridan, R. Meams, S. J. Stranick, W. F. Mitchell, L. C. Brinson, V. Gudapati, D. Hartman, A. Vaidya, J. W. Gilman and G. A. Holmes, *Compos. Sci. Technol.*, 2020, **192**, 1–8.
- 31 J. W. Woodcock, R. Beams, C. S. Davis, N. Chen, S. J. Stranick, D. U. Shah, F. Vollrath and J. W. Gilman, *Adv. Mater. Interfaces*, 2017, **4**, 1601018.
- 32 A. N. Gent and B. Park, *J. Mater. Sci.*, 1984, **19**, 1947–1956.

